

Spatially Inhomogeneous Impurity Distribution in ZnO Micropillars

Thomas Nobis,* Evgeni M. Kaidashev,† Andreas Rahm, Michael Lorenz, Jörg Lenzner, and Marius Grundmann

Universität Leipzig, Fakultät für Physik und Geowissenschaften, Institut für Experimentelle Physik II, Linnéstr. 5, D-04103 Leipzig, Germany

Received January 19, 2004; Revised Manuscript Received March 17, 2004

ABSTRACT

Using ZnO a variety of micro- and nanostructures can be fabricated. We investigate hexagonal micropillars grown by high pressure pulsed laser deposition on sapphire with spatially and spectrally resolved cathodoluminescence. We demonstrate that the impurity and defect incorporation is strongly inhomogeneous, at least under the present growth conditions, dramatically influencing the optical properties.

Advances of micro- and nanotechnology in electronics and photonics rely on the preparation of tailored structures. Recently a number of novel microstructured crystal geometries has been reported. The material that shows the widest range of structures seems to be currently ZnO, and, e.g., wires,¹ tubes,² belts,³ branched structures,⁴ nanonails,⁵ and even spirally wound rings,⁶ can be found in the literature. So far the optical properties of individual ZnO microcrystals have not been investigated for most structures. In this article we use spatially and spectrally resolved cathodoluminescence (CL) microscopy⁷ to investigate in detail the optical properties of zinc oxide micropillars, providing insight into the impurity and defect distribution.

A SEM-image of the investigated area of the sample is given in Figure 1. The microcrystals shown have been grown at 915 °C self-assembled on a-plane sapphire substrates by high-pressure pulsed laser deposition (PLD), similar to the method of Morales and Lieber.⁸ A KrF excimer laser was used to evaporate the ZnO target, and argon acted as transport gas within the PLD chamber. As growth catalyst, circular regions of the substrates were sputtered with a few nanometer thin gold film. Within these circles ZnO pillars of different diameter and height have grown, exhibiting a hexagonal footprint indicating the c-orientation of their wurtzite lattice. The crystals' diameters vary from 1 μm up to 5 μm, their heights differ in a range from 3 μm to 20 μm. More detailed information about this growth process will be published elsewhere.⁹

Room-temperature CL spectra have been collected in plan-view pointwise within the area marked in Figure 1 using a scan grid of 64 × 48 points. The pillars show two luminescence bands, the first around 3.23 eV (ultraviolet

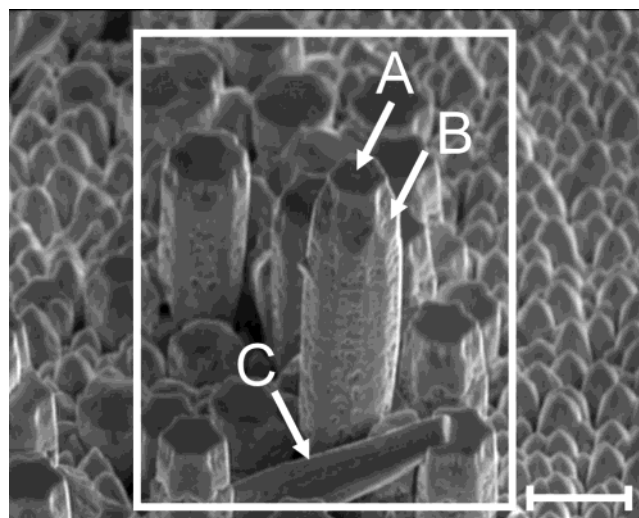


Figure 1. SEM-image of pillar-shaped ZnO microcrystals taken at $U = 10$ kV and observed from 45° perspective. CL-scan area is denoted by a white rectangle. The scale bar has a length of $5 \mu\text{m}$. Labels A and B mark the positions at which the spectra from Figure 3 were obtained. Letter C marks a strained micropillar described in Figure 5 below.

emission, UV range), the second around 2.35 eV (green or visible emission, VIS range), whose relative intensity varies spatially. While the first emission is associated with exciton emission, the second usually indicates recombination at deep levels, presumably caused by oxygen defects.¹⁰ To visualize the spatial variation between these two bands, the map of the intensity ratio

$$R(x,y) = \frac{I_{\text{UV}}(x,y)}{I_{\text{VIS}}(x,y)} \quad (1)$$

is shown in Figure 2. The numerator characterizes the

* Corresponding author. E-mail: nobis@physik.uni-leipzig.de.

† On leave from: Rostov-on-Don State University, Mechanics and Applied Mathematics Research Institute, 344090 Rostov-on-Don, Russia.

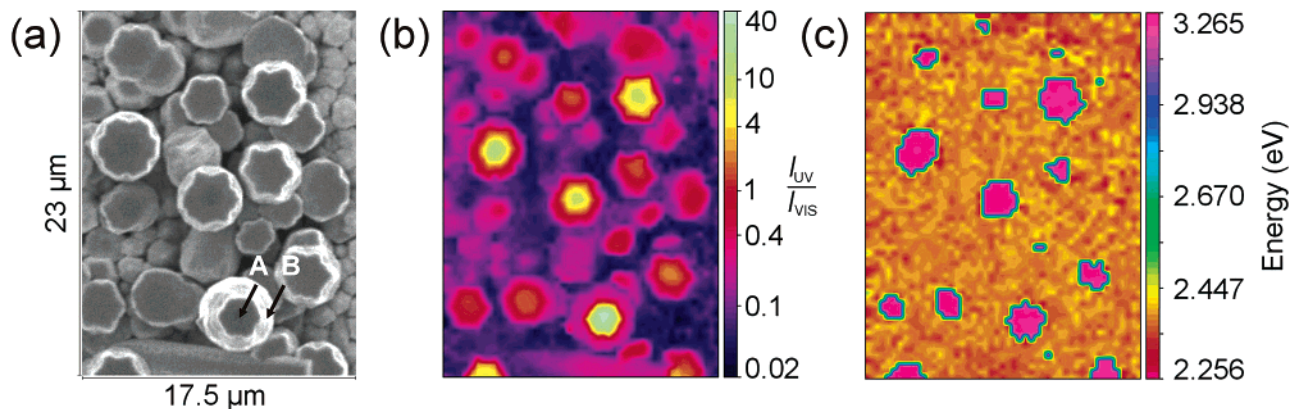


Figure 2. (a) SEM-image (top view) of the pillar structure. (b) Spatial map of the intensity ratio from eq 1 using a logarithmic color-scale. (c) Map of the spectral maximum.

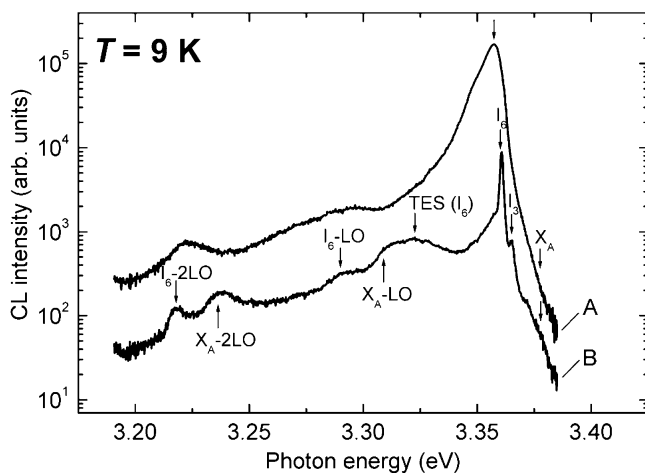


Figure 3. Local CL spectra at $T = 9$ K for the positions A and B as indicated in Figure 1 and Figure 2a.

integrated average UV luminescence intensity (3.0 eV to 3.35 eV), the denominator describes the same for green luminescence (1.7 eV to 2.85 eV). Also, a map of the spectral position of the peak maximum is given in Figure 2 in comparison with the simultaneously recorded SEM image.

As can be seen from the ratio map (Figure 2b), UV emission is extremely enhanced at all the pillars' centers (yellow regions), whereas visible emission is suppressed there. The maximum intensity ratio of around 40 is obtained at point A. When approaching the border of the pillars, the intensity ratio decreases below 0.1 and green emission dominates (violet and dark regions), indicating an increasing influence of point defects. The peak positions map underlines this fact, as in the center of the pillars the UV peak represents the global spectral maximum, whereas the green luminescence peak exceeds the UV peak near the border of the pillars and on the sample's bottom.

To reveal reasons for the enhanced UV luminescence intensity, highly resolved ($\Delta E = 0.9$ meV) low temperature ($T = 9$ K) CL spectra have been collected shown in Figure 3.

The spectrum from the border of the pillar at point B shows a dominating narrow line at 3.3607 eV (I_6), indicating a neutral donor bound exciton transition also typically

observed for our thermally grown ZnO nanowires¹¹ and PLD grown ZnO thin films on sapphire.¹² Meyer et al. identified this donor as aluminum.¹³ The fwhm of the (D^0, X) peak is 1.6 meV and thus comparable with literature values for single crystals and thin films.¹¹ Furthermore, a small line at 3.365 eV (I_3) is observable, presumably belonging to an ionized donor bound exciton.¹³ Phonon replica¹⁴ and two-electron satellites (TES) of the main peak can be found additionally. Free exciton emission (X_A) is more clearly resolved at higher temperatures. In comparison to point B, at point A the maximum UV intensity is about 20 times greater, as expected from the room temperature data, but the spectral maximum is additionally shifted by about 3 meV to lower energies (3.3575 eV) in association with a line broadening of about a factor of 6 (fwhm = 9.2 meV). A spectrum line scan across the top of the crystal (Figure 4) visualizes the spatial distribution of both observed lines in detail, particularly the occurrence of the lower energy line in the pillar center.

At the border of the pillar and near the edge of the hexagonal top only the narrow line I_6 occurs, whereas at the inner center the broad second line appears. The line shape of spot spectra could be modeled with a fixed Lorentzian line at 3.3607 eV, and a second broader Gaussian line with a varying peak position around 3.358 eV. In Figure 4c the fit position of the varying peak is plotted vs the spatial coordinate together with the I_6 peak position as long as I_6 could be observed. When approaching the center of the pillar, I_6 rapidly disappears and the second line increases in intensity and gradually shifts between 1 meV to 3 meV to lower energies. We therefore come to the conclusion that this line does not belong to an additional donor (gallium, I_8 or indium, I_9)¹³ since in that case it should arise at a spectrally fixed position.

Another potential reason of the observed effects could be an inhomogeneous strain distribution across the cross section of the pillars. Therefore, the observed red shift would have to be attributed to a *tensile* deformation of the pillar's core. A strain effect is observed for micropillar C of Figure 1 which came under compressive stress from neighboring pillars at their junction point. A continuous blue shift of the I_6 line by a few meV can be seen in Figure 5. In this case, however, the recorded line remains sharp. Such strain-

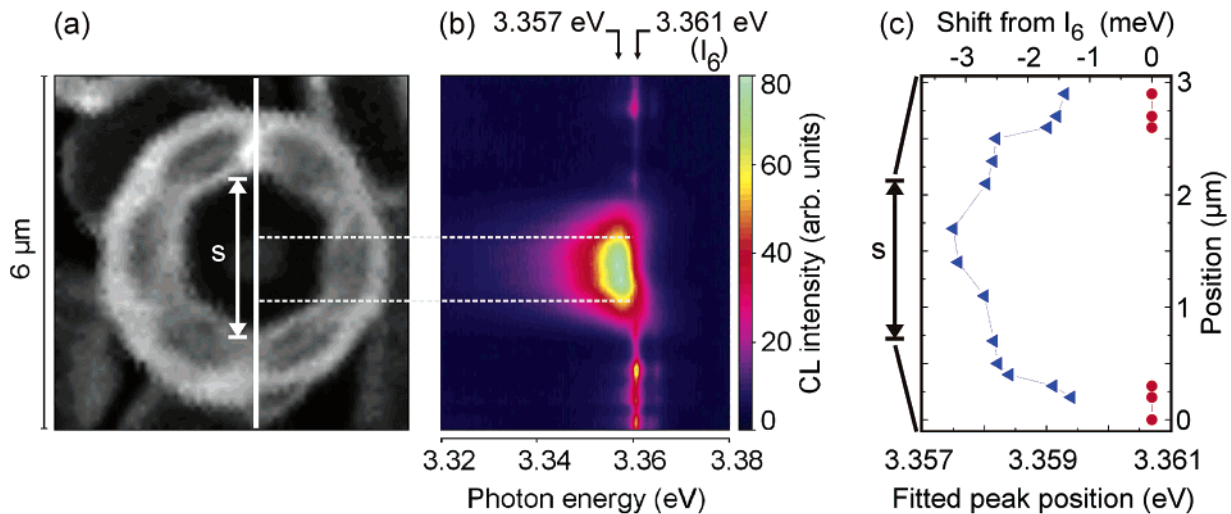


Figure 4. Line scan across the top of a microcrystal at $T = 9$ K. (a) Top view SEM image of the pillar at point A. The vertical white axis marks the chosen scan line. The section labeled with S refers to Figure 4c. (b) Spectral line scan along the white line in part 4a. The horizontal dashed white lines visualize the local restriction of the red shifted peak. (c) Fitted positions of both observed peaks in dependence of the spatial coordinate within the section S in Figure 4a. Red circles identify the I_6 peak, blue triangles describe the shifting lower energy peak.

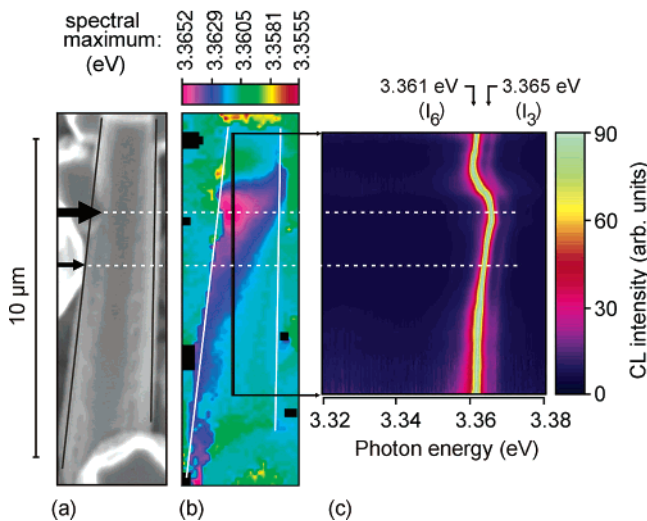


Figure 5. Strain distribution along the distorted micropillar C of Figure 1 recorded at $T = 9$ K. (a) Top view SEM image of the pillar. Vertical black lines mark the pillar's position, black arrows indicate the points at which the pillar is set under pressure by neighboring crystals. (b) Map of the spectral maximum within the UV range. When approaching the positions marked by the horizontal dashed white lines, the I_6 peak shifts to higher energies according to a compressive strain. (c) Spectral line scan along the vertical black line in Figure 5b, all spectra are scaled to the same total intensity. The spectral range is the same as in Figure 4b. In strained regions of the crystal the I_6 line continuously shifts to higher energies and remains sharp. Additionally, one can see as a thin violet curve the simultaneously shifting I_3 peak accompanying the winding yellow I_6 line at a constant energy separation of 4 meV.

induced shift corresponds to a strain in the 10^{-3} regime, the exact value depending on the symmetry of the strain. The experiment on the standing pillars shows that the outer regions are anyway *unstrained*, since the I_6 line at the pillars' margins appears neither shifted nor broadened compared to its properties in bulk material. In addition, transmission electron microscopy investigations¹⁵ on similar samples

furthermore show a growth free of extended defects such as dislocations or stacking faults, especially at the crystals' centers. Thus an inhomogeneous broadening of the luminescence lines cannot be attributed to structural defects. Moreover, it is highly unlikely that strain or structural defects would *increase* the CL intensity within the range of donor-bound exciton transitions by a factor of 20. Therefore, we also exclude strain as a cause of the shift in Figure 4. We note that in a number of thin film samples with slightly varying residual strain we find the I_6 line to vary systematically with the lattice constant by a few meV and to remain sharp.

We propose that a strong accumulation of Al occurs in the center of the pillars. An increased level of Al has been actually found by local EDX analysis in TEM investigations.¹⁵ This simultaneously explains both the increased luminescence intensity *and* the broad line shape. High doping concentrations can cause a red shift of donor bound exciton lines, as already known for nitrogen-bound excitons in GaP.¹⁶ Moreover, when doping ZnO with gallium Ko et al.¹⁷ found the Ga-related peak red shifted from I_8 by about 2 meV for $N_D = 5.7 \times 10^{18} \text{ cm}^{-3}$. Hence, we assume that our experiments indicate the local concentration and accumulation of aluminum at the center of the studied ZnO pillars. The reason for the accumulation cannot be unambiguously revealed by the present investigations. It could possibly originate from the Al_2O_3 substrate and reach the pillars' tops by a diffusion process. Another possible scenario is the following: as mentioned before, the substrate has been sputtered by a thin gold film before the growth process and has afterward been heated to the growth temperature of above 900 °C. Possibly a high amount of Al from the substrate has been solved within the gold that had melted while heating. This aluminum could have been deposited over the cross section of the pillar while growing. Additionally, the final growth stage possibly runs in a core-shell manner with

the outer layers exhibiting smaller Al concentration because the sapphire substrate becomes completely covered during growth and/or the gold drop has exhausted its aluminum. Possibly the surface layers exhibit different structural properties (e.g., higher vacancy content as evidenced by the VIS recombination) and suffer less aluminum diffusion or incorporation than the core.

In summary, our investigations show that donor and defect distributions in ZnO microcrystals grown at high temperature directly on sapphire substrates can be profoundly inhomogeneous, influencing the local optical properties dramatically. Further work such as annealing experiments and variation of growth conditions are planned. The high Al content in the core of the microcrystals is expected to make them conductive and therefore attractive for electric applications, which will be subject to further investigations.

Acknowledgment. This work was supported by Deutsche Forschungsgemeinschaft within FOR 522 (Project Gr 1011/

12-1). We thank G. Wagner for TEM analysis of ZnO microcrystals.

References

- (1) Yang, P. et al. *Adv. Funct. Mater.* **2002**, *12*, 323–331.
- (2) Vayssieres, L. et al. *Chem. Mater.* **2001**, *13*, 4395–4398.
- (3) Wang, Z. L. *Adv. Mater.* **2003**, *15*, 432–436.
- (4) Lao, J. Y. et al. *Nano Lett.* **2002**, *2*, 1287–1291.
- (5) Lao, J. Y. et al. *Nano Lett.* **2003**, *3*, 235–238.
- (6) Korgel, B. A. *Science* **2004**, *303*, 1308–1309.
- (7) Christen, J. et al. *J. Vac. Sci. Technol. B* **1991**, *4*, 2358–2368.
- (8) Morales, A. M.; Lieber, C. M. *Science* **1998**, *279*, 208–211.
- (9) Lorenz, M. et al., unpublished.
- (10) Lin, B. et al. *Appl. Phys. Lett.* **2001**, *79*, 943–945.
- (11) Lorenz, M. et al. *Ann. Phys.* **2004**, *13*, 39–42.
- (12) Kaidashev, E. M. et al. *Appl. Phys. Lett.* **2003**, *82*, 3901–3903.
- (13) Meyer, B. K. et al. *Phys. Status Solidi B* **2004**, *241*, 231–260.
- (14) Ashkenov, N. et al. *J. Appl. Phys.* **2003**, *93*, 126–133.
- (15) Lorenz, M. et al. unpublished.
- (16) Thomas, D. G.; Hopfield, J. J. *Phys. Rev.* **1966**, *150*, 680–689.
- (17) Ko, H. J. *Appl. Phys. Lett.* **2000**, *77*, 3761–3763.

NL049889Y